^{7,9,10}Be elastic scattering and total reaction cross sections on a ^{12}C target

J. C. Zamora,[1] V. Guimarães,[1] A. Barioni,[1] A. Lépine-Szily,[1] R. Lichtenthäler,[1] P. N. de Faria,[1] D. R. Mendes Jr.,[1] L. R. Gasques,[1] J. M. B. Shorto,[2] V. Scarduelli,[1] K. C. C. Pires,[1] V. Morcelle,[1] E. Leistenschneider,[1] R. P. Condori,[1] V. A. Zagatto,[1] M. C. Morais,[1] and E. Crema[1]

[1]*Instituto de Física, Universidade de São Paulo, P.O. Box 66318, 05389-970 São Paulo, SP, Brazil*

[2]*Instituto de Pesquisas Energéticas e Nucleares, IPEN-CNEN, São Paulo, SP, Brazil*

(Received 4 August 2011; published 21 September 2011)

Elastic scattering angular distributions for ^{7}Be, ^{9}Be, and ^{10}Be isotopes on ^{12}C target were measured at laboratory energies of 18.8, 26.0, and 23.2 MeV, respectively. The analysis was performed in terms of optical model potentials using Woods-Saxon and double-folding form factors. Also, continuum discretized coupled-channels calculations were performed for ^{7}Be and ^{9}Be $+$ ^{12}C systems to infer the role of breakup in the elastic scattering. For the ^{10}Be $+$ ^{12}C system, bound states coupled-channels calculations were considered. Moreover, total reaction cross sections were deduced from the elastic scattering analysis and compared with published data on other weakly and tightly bound projectiles elastically scattered on the ^{12}C target, as a function of energy.

DOI: 10.1103/PhysRevC.84.034611 PACS number(s): 25.60.Bx, 25.70.Bc, 25.60.Gc, 24.10.Eq

I. INTRODUCTION

A topic of great interest in nuclear physics research nowadays is the study of properties of proton- or neutron-rich nuclei, i.e., those far from the stability line. An important tool to investigate these nuclei is elastic scattering on light and heavy targets. Elastic scattering has been used extensively to investigate the inner structure and the influence of different reaction mechanisms of several systems that involve unstable weakly bound nuclei [1–6]. Due to the lower binding energy of these nuclei, breakup can become an important competing process even at relatively low incident energies, and a coupled-channels analysis is required. Thus, from a complete analysis of the elastic scattering, important information of other reaction channels can be obtained. Also, from an optical-model analysis of the elastic scattering, the total reaction cross section can be deduced. Recently, several systematics of total reaction cross section have been reported in the literature with the aim of investigating how the dynamic, static, and geometrical effects of the projectile influence the reaction channels [7–11].

In this paper we report measurements of elastic scattering of ^{7}Be, ^{9}Be, and ^{10}Be on a natural carbon target. The main goal of these measurements is to investigate the importance of breakup on the scattering of the weakly bound isotopes ^{7}Be and ^{9}Be on a light target in comparison with the strongly bound unstable ^{10}Be isotope. To investigate the influence of dynamic effects on systems with these beryllium projectiles, we performed a systematics involving many other stable and unstable, tightly and weakly bound light projectiles, all scattered on a carbon target.

The organization of this paper is the following. Section II describes the experimental and detection setups used. Section III exhibits the experimental results and the theoretical analysis with optical-model and coupled-channels calculations. The comparison of reduced total reaction cross sections for many systems is also presented in this section. We present a summary of the results and the conclusions for this study in Sec. IV.

II. THE EXPERIMENT

Elastic scattering angular distributions of the beryllium isotopes, ^{7,9,10}Be, on a natural carbon target were measured at $E_{\rm lab} = 18.8$, 26.0, and 23.2 MeV, respectively. These angular distributions were obtained using secondary radioactive beams produced by the RIBRAS facility [12] at the Universidade de São Paulo, Brazil. In this facility, radioactive ion beams are produced in-flight from transfer reactions between a stable accelerated beam and a light target. The secondary radioactive beam is selected and focused by a strong magnetic field ($B_{\rm max} = 6.5$ T) from a superconductor solenoid with angular acceptance ranging from 2° to 6°. The ^{7}Be ion beam was obtained by impinging a 28-MeV primary beam of ^{6}Li^{3+} on a ^{3}He gas target kept at 1 atm pressure. The ^{10}Be beam was produced by a ^{11}B^{5+} primary beam of 35 MeV on a ^{9}Be target 12 μm in thickness. Due to the fact that particles with the same magnetic rigidity can be selected together with the beam of interest, the ^{9}Be beam was also obtained as a contaminant of the ^{10}Be beam.

After passing through the production target, primary beams are stopped in a Faraday cup, which integrates the charge and allows the measurement of their intensities (about 200 e nA). For each 1 μA of primary beam, the secondary beam intensities of ^{7}Be, ^{9}Be, and ^{10}Be were 4×10^{5}, 5×10^{3}, and 2×10^{3} pps, respectively. The secondary beams were collected and focused on the reaction targets, ^{12}C (1.05 mg/cm^2 in thickness) and gold (5.29 mg/cm^2 in thickness), which were used in separate runs to obtain the overall normalization.

The elastic scattered particles were identified by three ΔE-E (telescope) silicon detectors, placed at different angles. The ΔE detector of 20 μm in thickness and 300 mm^2 in area was backed by the E detector of 1000 μm in thickness. These telescopes had collimators with apertures that subtended solid angles of about 12 msr. The energy resolution of the detectors ranged from 5% to 8% for detected particles. Typical ΔE-E particle identification spectra can be seen in Figs. 1 and 2.

The angular distributions were measured over an angular range of 15° to 60° in the laboratory frame. A correction to the

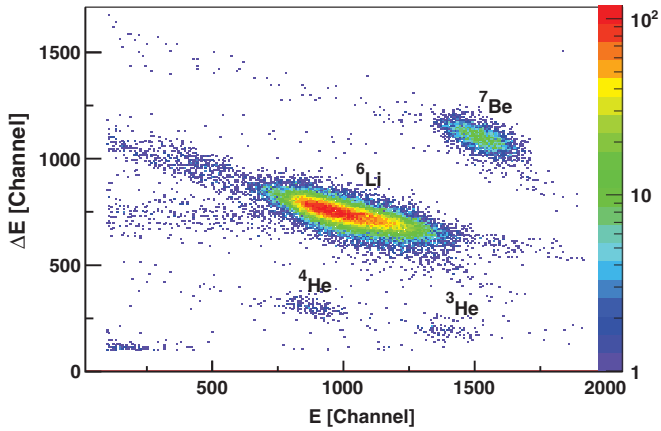

FIG. 1. (Color online) Particle identification ΔE-E spectrum of elastic scattered particles on gold target at 15°. The ^{7}Be and the contaminant ^{6}Li, ^{4}He, and ^{3}He particles are identified.

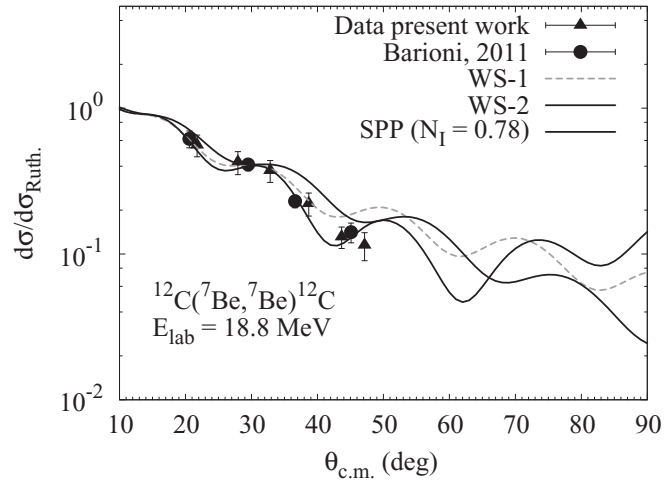

FIG. 3. Differential cross section for the elastic scattering of the ^{12}C(^{7}Be,^{7}Be)^{12}C system. The experimental data are from the present work and from Barioni *et al.* [11]. The lines refer to calculations with Woods-Saxon and double-folding potentials as indicated. See text for details.

average angle of detection was necessary due to the angular aperture of the collimators of the telescopes (about 5° to 6° in the laboratory system, which corresponds to almost 10° in the center of mass system). This correction was made using a Monte Carlo simulation program that takes into account the effective area of the detector, the radius, and the divergence of the secondary beam and also the angular straggling of the beam as it passes through the target.

The experimental differential cross sections for the beryllium isotopes can be seen in Figs. 3, 4, and 5. The uncertainties in differential cross section were calculated by considering the statistical uncertainty in the yield, the uncertainty in the secondary beam intensity (about 15%), the uncertainty in the number of particles in the targets (1%), and the uncertainty in the solid angle (2%).

III. ANALYSIS

To complement the experimental angular distributions for ^{7}Be and ^{9}Be, data from previous experiments from Ref. [11] for ^{7}Be and Ref. [13] for ^{9}Be measured at the same energies were also considered. For ^{10}Be + ^{12}C, the elastic scattering has been measured for the first time at low energy. Theoretical analysis of the present angular distributions was performed with the code FRESCO [14] and is divided in three parts: optical-model (OM) calculations, coupled-channels calculation, and a systematics of the total reaction cross section of several light projectiles scattered on a ^{12}C target.

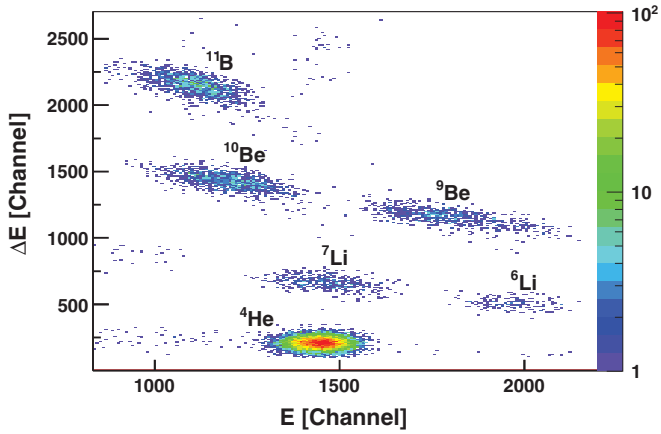

FIG. 2. (Color online) Particle identification ΔE-E spectrum of elastic scattered particles on gold target at 15°. The ^{10}Be and the contaminant ^{9}Be particles of interest are identified as well as the other ^{11}B, ^{7}Li, ^{6}Li, and ^{4}He contaminants.

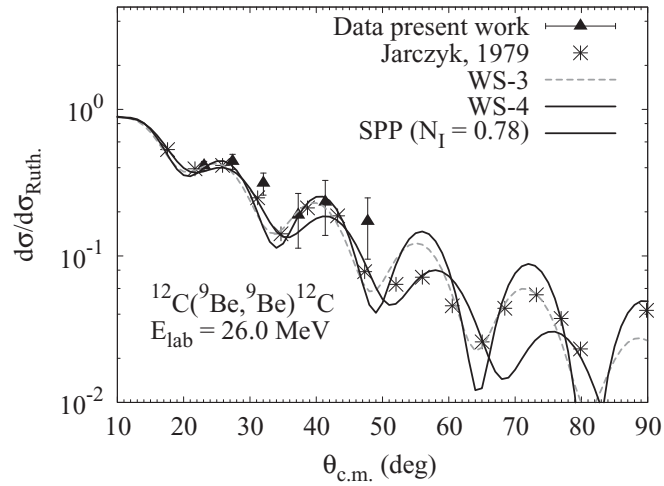

FIG. 4. Differential cross section for the elastic scattering of the ^{12}C(^{9}Be,^{9}Be)^{12}C system. The experimental data are from the present work and from Jarczyk *et al.* [13]. The lines refer to calculations with Woods-Saxon and double-folding potentials as indicated.

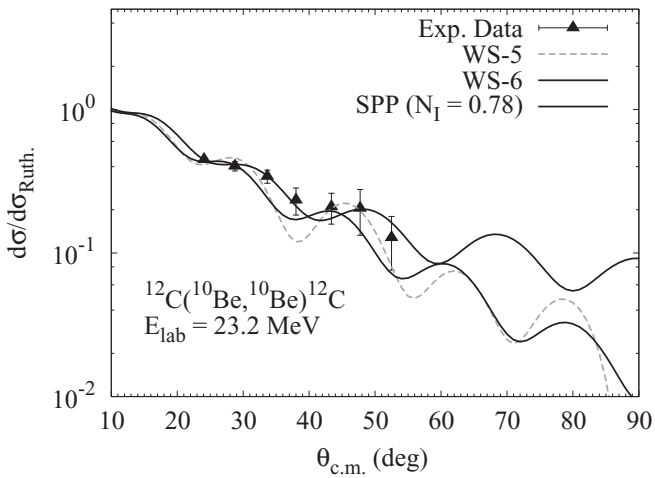

FIG. 5. Differential cross section for the elastic scattering of the ^{12}C(^{10}Be,^{10}Be)^{12}C system. The lines refer to calculations with Woods-Saxon and double-folding potentials as indicated.

A. Optical-model calculations

The OM analyses were carried out in terms of both volume type Woods-Saxon (WS) and São Paulo double-folding (SPP) potentials. The SPP is an energy-dependent double-folding potential that takes into account the effects of Pauli nonlocality due to exchange between nucleons from the projectile and the target [15]. The nuclear densities used to determine this potential come from average values obtained from electron scattering data and calculations with the Dirac-Hartree-Bogoliubov approximation. Within the context of OM analysis the imaginary potential can be obtained as a normalization factor multiplied by the real potential (V_{SPP}):

$$V_{OM} = V_{SPP}(1 + iN_I). \quad (1)$$

The normalization factor employed to analyze the present systems is $N_I = 0.78$, which was obtained from an analysis of elastic scattering data using the optical potential of Eq. (1) in multiple systems [16]. The WS optical potentials considered in our calculations were obtained from other works with projectiles of similar mass on a carbon target. The parameters of each potential can be seen in Table I. Also, optical potential (WS) parameters were obtained from a fitting of the ^{7}Be and ^{10}Be angular distributions. Although a better description of the angular distribution is achieved for the parameters from the fitted angular distributions, all potentials give similar total reaction cross sections, also listed in Table I. The results of the optical-model analysis can be seen in Figs. 3, 4, and 5. The WS potentials considered give a good description of the data at forward angles. The SPP, which can be considered as a bare potential, also gives a reasonable description of the data at forward angles, but fails to reproduce backward angles, indicating the possible importance of other reaction channels.

B. Coupled-channels calculations

To verify the influence of any other reaction channel on the elastic scattering we refined the analysis by considering coupled-channels calculations. Continuum discretized coupled-channels (CDCC) calculations were performed for the weakly bound isotopes ^{7}Be (B.E. = 1.59 MeV) and ^{9}Be (B.E. = 1.67 MeV) as the breakup may be an important reaction channel. For the tightly bound ^{10}Be, only the two first bound states' channels were coupled.

The starting point of the CDCC calculation is to adopt the cluster-folding model to describe the interaction between the projectile and the target, and thus the ^{7}Be was considered a ^{4}He + ^{3}He cluster, with a binding energy of 1.59 MeV. The coupling to the continuum was made up to an excitation energy of $\epsilon_{max} = 5$ MeV above the threshold and was divided in bins of angular momenta $\ell = 0$, 1, and 2 $\hbar$. The width of the bins was $\Gamma = 0.5$ MeV for angular momentum $\ell = 0$ and $\Gamma = 1.0$ MeV for the other values of ℓ. The interaction between the core and the target (^{4}He + ^{12}C) was described by the SPP, whereas the fragment-target (^{3}He + ^{12}C) interaction was outlined by the Woods-Saxon optical potential from Ref. [18]. To describe the core-fragment (^{3}He + ^{4}He) interaction, a real WS potential was adopted with radius parameter $R = 1.2(3^{1/3} + 4^{1/3})$ fm and diffuseness parameter $a = 0.56$ fm, similar to the parameters in Ref. [19]. These potentials are shown in Table I. As one can see in Fig. 6, both CDCC and cluster-folding model potential calculations (no couplings)

TABLE I. Optical-model potential parameters used in the calculations. Radii are given by $R_x = r_x \times (A_P^{1/3} + A_T^{1/3})$. The depths are in MeV, the radii and diffuseness in fm, and the cross sections in mb.

Potential	V	r_V	a_V	W	r_W	a_W	r_C	σ_R	Reference
WS-1	33.69	1.00	0.92	6.53	1.56	0.49	0.65	1278	^{9}Be + ^{12}C [17]
WS-2	94.18	1.26	0.60	59.84	1.48	0.20	1.48	1224	This work
WS-3	60.00	1.18	0.60	32.60	1.18	0.60	0.63	1428	^{9}Be + ^{12}C [13]
WS-4	100.00	1.23	0.48	17.00	1.30	0.26	1.45	1327	^{11}B + ^{12}C [18]
WS-5	100.00	1.15	0.50	10.00	1.30	0.22	1.40	1182	^{10}B + ^{12}C [18]
WS-6	32.35	0.89	0.85	5.77	1.37	0.36	0.62	1004	This work
^{3}He + ^{4}He (CDCC)	110.00	1.20	0.56						This work
n + ^{8}Be (CDCC)	110.00	1.20	0.40						This work
	V	r_V	W	r_W	V_{so}	r_{so}	a_x	r_C	
^{3}He + ^{12}C (CDCC)	125.40	0.74	12.50	0.74			0.69	0.86	[18]
n + ^{12}C (CDCC)	48.00	0.97	3.20	0.73	5.50	0.84	0.4		[18]

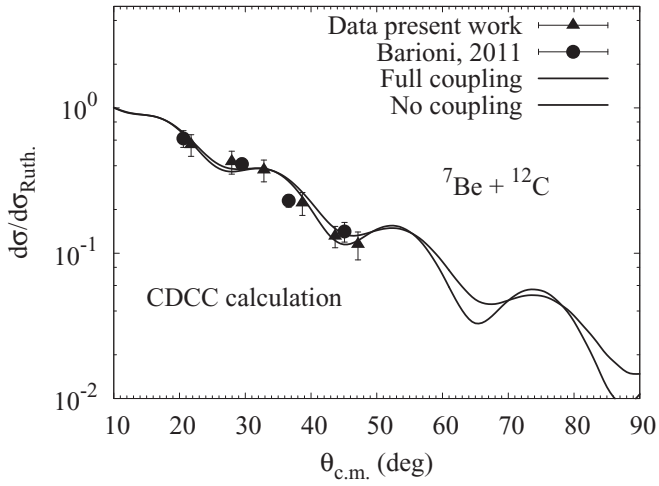

FIG. 6. Differential cross section for the elastic scattering of the ^{12}C(^{7}Be,^{7}Be)^{12}C system. The experimental data are from the present work and from Barioni *et al.* [11]. The solid line is the result of the CDCC calculation and the dashed line is the cluster-folding parametrization with no couplings to the continuum.

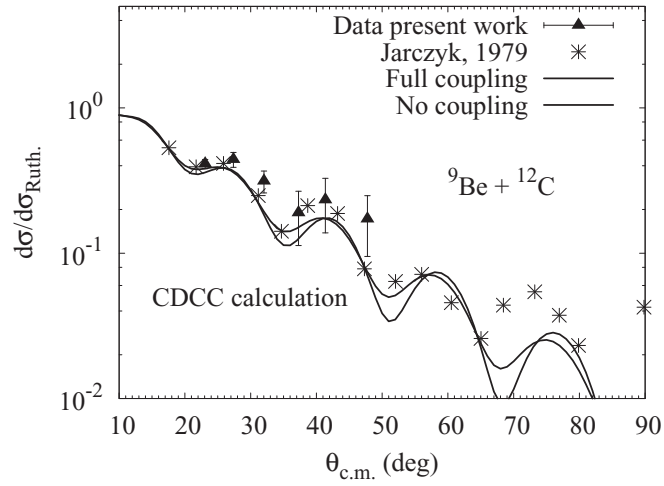

FIG. 7. Differential cross section for the elastic scattering of the ^{12}C(^{9}Be,^{9}Be)^{12}C system. The experimental data are from the present work and from Jarczyk *et al.* [13]. The solid line is the result of the CDCC calculation and the dashed line is the cluster-folding parametrization with no couplings to the continuum.

describe very well the experimental angular distribution and the effects of the coupling is rather small.

The stable weakly bound ^{9}Be isotope was considered to have a ^{8}Be + n cluster configuration. In this representation, the three-body CDCC calculation has been providing good results in other systems [20,21], although the core particle is not bound. For the present calculation, special attention was given to the continuum discretization of the ^{9}Be nucleus because it has many resonances. In particular, the resonances $1/2^{+}$, $5/2^{-}$, $5/2^{+}$, and $3/2^{-}$ in ^{9}Be were considered as bins centered at their respective energies. The couplings to the continuum were made up to an energy of $\epsilon_{max} = 8$ MeV above the threshold and divided in bins of angular momenta $\ell = 0$, 1, 2, and 3 $\hbar$. Similar to the calculation for ^{7}Be, the interaction core-target (^{8}Be + ^{12}C) was described by the SPP. The parameters for the fragment-target (n + ^{12}C) and core-fragment (n + ^{8}Be) potentials are listed in Table I, including a spin-orbit term considered for the fragment-target interaction. The calculated angular distribution reproduces reasonably the data up to an angle of 65°, as shown in Fig. 7. The coupling to the continuum has a small contribution to the elastic scattering as can be seen by comparison with the no-coupling calculation.

The ^{10}Be is a tightly bound nucleus with a neutron separation energy of B.E. = 6.81 MeV. Due to this high binding energy, the Coulomb dissociation channel should not play an important role for this system. Therefore, to describe the experimental angular distribution, we have performed coupled-channels calculations including the 2_1^+ and 0_1^+ bound states. These excited states correspond to the two most probable quadrupolar transitions in ^{10}Be [22]. For the analysis, we adopted the vibrational model of two phonon states with reduced transition probabilities $B(E2)(2_1^+ \rightarrow 0_{gs}^+) = 8.0$ W.u. and $B(E2)(0_1^+ \rightarrow 2_1^+) = 2.5$ W.u., taken from Ref. [23]. The results of such calculations are shown in Fig. 8. In this figure, the bare potential corresponds to a complex potential with the real part given by SPP and the imaginary part as a short-range Woods-Saxon potential with parameters taken from Ref. [24], $V = 80$ MeV, $R = 0.8$ fm, and $a = 0.6$ fm. This short-range potential is used to not disturb the competition between the surface channels and to take into account the effects of the fusion channel. It simulates the boundary conditions of the incoming wave and its parameters do not have a large influence on later calculations [25,26]. By including the first excited state (2_1^+) the bare distribution is strongly affected and it is possible to see the loss of flux of the elastic channel. The inclusion of the second excited state does not change very much the calculated angular distribution, which demonstrates that the first excited state is the most important inelastic

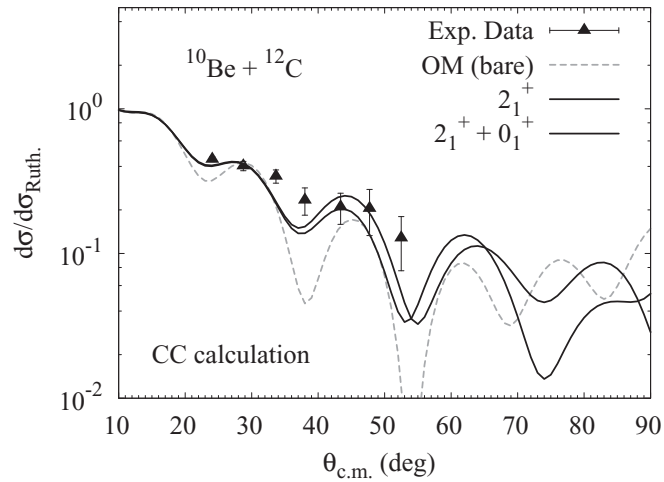

FIG. 8. Differential cross section for the elastic scattering of ^{12}C(^{10}Be,^{10}Be)^{12}C system. The dashed line corresponds to calculations with the bare potential. The dotted line is the result after including the first excited state 2_1^+ and the solid line corresponds to the results after including the first and second excited states, 2_1^+ and 0_1^+.

TABLE II. Data and parameters used to determine the total reaction function $F(x)$ and reduced reaction cross sections as described in the text. The energies, potentials, and $\hbar\omega_0$ are in MeV, the radii in fm, and the cross sections in mb.

System	$E_{\text{c.m.}}$	R_B	V_B	$\hbar\omega_0$	σ_R	x	$F(x)$	Ref.
^{4}He + ^{12}C	8.81	6.90	2.34	4.15	591	1.56	5.26	[34]
^{4}He + ^{12}C	9.35	6.90	2.34	4.15	572	1.69	5.41	[34]
^{4}He + ^{12}C	10.50	6.90	2.34	4.15	597	1.97	6.34	[34]
^{4}He + ^{12}C	12.00	6.90	2.34	4.15	735	2.33	8.92	[34]
^{4}He + ^{12}C	13.50	6.90	2.34	4.15	813	2.69	11.10	[34]
^{4}He + ^{12}C	14.25	6.90	2.34	4.15	810	2.87	11.68	[34]
^{6}He + ^{12}C	5.99	7.97	2.04	3.30	1285	1.20	7.36	[31]
^{6}He + ^{12}C	6.60	7.97	2.04	3.30	1168	1.38	7.36	[30]
^{6}He + ^{12}C	12.00	7.97	2.04	3.30	1521	3.02	17.44	[10]
^{6}Li + ^{12}C	3.00	7.52	3.37	3.93	107	−0.10	0.29	[27]
^{6}Li + ^{12}C	6.00	7.54	3.33	3.93	811	0.68	4.36	[28]
^{6}Li + ^{12}C	7.30	7.55	3.33	3.91	962	1.01	6.30	[28]
^{6}Li + ^{12}C	16.00	7.59	3.24	3.81	1307	3.35	19.08	[29]
^{6}Li + ^{12}C	20.00	7.67	3.13	3.82	1366	4.42	24.32	[29]
^{7}Li + ^{12}C	2.84	7.57	3.34	3.82	67	−0.13	0.17	[27]
^{7}Li + ^{12}C	6.95	7.76	3.17	4.08	1004	0.93	5.68	[28]
^{7}Li + ^{12}C	8.21	7.76	3.17	4.08	1103	1.23	7.37	[28]
^{7}Li + ^{12}C	9.47	7.76	3.17	4.08	1170	1.54	9.02	[28]
^{7}Li + ^{12}C	13.26	7.76	3.17	4.08	1275	2.47	13.76	[28]
^{8}Li + ^{12}C	14.34	8.03	2.97	2.91	1605	3.90	24.50	[4]
^{7}Be + ^{12}C	11.87	7.77	4.11	2.69	1198	2.89	17.54	This work
^{9}Be + ^{12}C	12.00	8.05	3.92	5.07	1334	1.59	9.75	[13]
^{9}Be + ^{12}C	14.90	7.98	3.99	3.03	1436	3.60	22.19	This work

TABLE III. Data and parameters used to determine the total reaction function $F(x)$ and reduced reaction cross sections as described in the text. The energies, potentials, and $\hbar\omega_0$ are in MeV, the radii in fm, and the cross sections in mb.

System	$E_{\text{c.m.}}$	R_B	V_B	$\hbar\omega_0$	σ_R	x	$F(x)$	Ref.
^{10}Be + ^{12}C	12.66	7.98	4.05	3.96	1197	2.17	12.01	This work
^{8}B + ^{12}C	15.48	7.74	5.16	2.80	1282	3.69	23.67	[11]
^{11}B + ^{12}C	5.40	7.82	5.29	3.97	164	0.03	0.73	[32]
^{11}B + ^{12}C	6.50	7.83	5.28	4.05	395	0.30	2.07	[32]
^{11}B + ^{12}C	7.20	7.83	5.28	4.08	527	0.47	3.03	[32]
^{11}B + ^{12}C	8.10	7.84	5.28	4.12	667	0.69	4.27	[32]
^{11}B + ^{12}C	8.60	7.84	5.27	4.14	734	0.80	4.96	[32]
^{11}B + ^{12}C	9.60	7.85	5.27	4.19	842	1.03	6.27	[32]
^{11}B + ^{12}C	10.50	7.85	5.27	4.23	1128	1.24	9.09	[32]
^{11}B + ^{12}C	11.50	7.86	5.26	4.25	993	1.47	8.69	[32]
^{11}B + ^{12}C	13.00	7.86	5.25	4.33	1081	1.79	10.51	[32]
^{11}B + ^{12}C	20.90	7.90	5.22	4.65	1320	3.37	19.01	[32]
^{11}B + ^{12}C	25.57	7.80	5.17	3.30	1413	6.18	35.96	[33]
^{12}C + ^{12}C	14.56	8.13	6.03	3.38	870	2.52	11.33	[35]
^{12}C + ^{12}C	16.02	8.13	6.03	3.38	871	2.95	12.48	[35]
^{12}C + ^{12}C	17.36	8.13	6.03	3.38	899	3.35	13.96	[35]
^{12}C + ^{12}C	18.30	8.13	6.03	3.38	932	3.63	15.26	[35]
^{12}C + ^{12}C	19.62	8.13	6.03	3.38	927	4.02	16.26	[35]
^{12}C + ^{12}C	20.75	8.13	6.03	3.38	931	4.35	17.28	[35]
^{12}C + ^{12}C	22.76	8.13	6.03	3.38	878	4.94	17.86	[35]
^{12}C + ^{12}C	26.24	8.13	6.03	3.38	955	5.97	22.42	[35]
^{12}C + ^{12}C	28.04	8.13	6.03	3.38	875	6.51	21.94	[35]
^{12}C + ^{12}C	30.90	8.13	6.03	3.38	909	7.35	25.12	[35]

channel to describe the elastic scattering of the ^{10}Be + ^{12}C system at the present energy.

C. Total reaction cross sections

From the analysis of the elastic scattering angular distributions it is also possible to deduce the total reaction cross sections. The total reaction cross sections for ^{7}Be, ^{9}Be, and ^{10}Be + ^{12}C obtained from the coupled-channels analysis are listed in Tables II and III together with the values obtained from other works with systems of light projectiles on ^{12}C. Among these systems we have combinations of weakly bound ^{6}Li [27–29], ^{7}Li [27,28], ^{8}Li [4], and ^{9}Be [13]; exotic nuclei ^{6}He [10,30,31] and ^{8}B [11]; and tightly bound ^{11}B [32,33] projectiles. We also included the total reaction cross section for α-cluster nuclei ^{4}He [34] and ^{12}C [35]. To compare the total reaction cross sections for different systems, it is important to reduce properly the data to reveal the role of static or dynamic effects on the reaction channels. The halo nuclei, for example, have a longer radial extension that reduces the Coulomb barrier causing the enhancement of transfer or fusion channels. On the other hand, the dynamic effects on weakly bound nuclei can affect the total reaction cross section due to the importance of the breakup and transfer mechanisms.

In this work we considered the reduction procedure proposed by Canto *et al.* [8], which was modified by Shorto *et al.* [9] by replacing fusion cross section (σ_f) for the total reaction cross section (σ_R), i.e.,

$$x = \frac{E - V_B}{\hbar\omega_0} \quad \text{and} \quad F(x) = \frac{2E}{\hbar\omega_0 R_B^2}\sigma_R. \tag{2}$$

The parameters V_B, R_B, and $\hbar\omega_0$ were determined by a parabolic fit of the real part of the optical potential obtained in the original works of each system listed in Tables II and III, with a radius close to the Coulomb barrier radii [9]. Here, x is the reduced energy and $F(x)$ is called the total reaction function because it is related to the total reaction cross section instead of the fusion cross section as in Ref. [8]. In principle, this procedure eliminates the geometrical and static effects, with only the dynamic ones of each system remaining. We can compare these results with Wong's [36] dimensionless equation

$$F_0(x) = \ln[1 + e^{(2\pi x)}], \tag{3}$$

also called the universal fusion function. The systematics for the different light projectiles scattered on the carbon target are shown in Fig. 9. All systems, excluding those involving ^{4}He and ^{12}C, follow the same trend guided by the universal fusion function. This behavior differs from that observed for weakly bound projectiles on heavy targets [8,9], where an enhancement of the total reaction cross sections at near barrier energies was observed. Therefore, in the present case, it is possible to infer that dynamic effects have a small influence on the reaction channels of weakly bound nuclei on light target, compared to halo projectiles (^{6}He and ^{8}B). Also, since the trend of reduced reaction cross sections is the same for more strongly bound projectiles, such as ^{10}Be and ^{11}B, and for exotic nuclei such as ^{6}He and ^{8}B, we can conclude that the

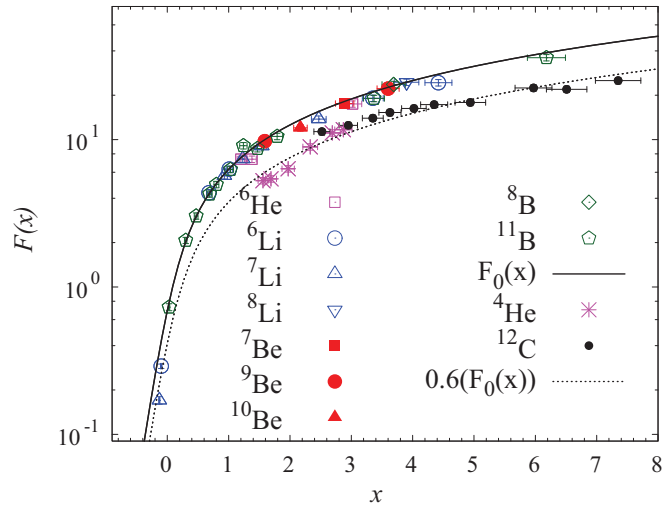

FIG. 9. (Color online) Reduced total reaction cross section systematics for several light beams scattered on a carbon target. The parameters are listed in Tables II and III.

Coulomb and nuclear breakup do not affect very much the total reaction cross sections for these light systems. Similar results were obtained when we considered the CDCC calculation. On the other hand, systems formed by α-cluster projectiles (^{4}He and ^{12}C) have smaller reduced total reaction cross sections in comparison with those of the other systems presented in Fig. 9. These nuclei have a high separation energy (for proton or neutron), which may quench reaction channels such as transfer. To quantify the lowering of the reduced total reaction cross sections for these nuclei we have multiplied the universal fusion function [$F_0(x)$] by a constant $k = 0.6$. Therefore, the reduced reaction cross section for ^{4}He and ^{12}C + ^{12}C systems are about 40% lower than the results obtained for the other reactions studied in this work.

IV. SUMMARY

We report here the study of elastic scattering angular distributions for ^{7}Be, ^{9}Be, and ^{10}Be on a carbon target. The analyses were performed in terms of an OM with WS and SPP potentials. From these analyses we can conclude that the WS optical potential can describe quite well our systems. Also, the SPP potential with $N_i = 0.78$ describes reasonably all the angular distributions.

To obtain information on other important reaction mechanisms, a detailed analysis with coupled-channels calculations was performed for each system. CDCC calculations were performed for the weakly bound ^{7}Be and ^{9}Be isotopes. From this analysis we conclude that the Coulomb and nuclear breakup effects are not relevant for these light systems on the light target ^{12}C. For ^{10}Be, which is a tightly bound nucleus, the elastic angular distribution was analyzed coupling the first two bound states, which involve quadrupolar transitions. In this analysis, it was shown that by only including a short-range imaginary bare potential (to account for the fusion channel) and the coupling to the bound states, it was possible to describe the experimental angular data for the ^{10}Be + ^{12}C system.

We also deduced from the elastic data the total reaction cross sections and compared them with values from several light projectiles elastically scattered on a carbon target. The total reaction cross sections were reduced in terms of the total reaction function to compare the influence of the coupled-channels on the different systems. From this systematics we can derive two interesting conclusions: weakly bound nuclei scattered on light targets do not have an important enhancement in the total reaction cross section (due to dynamic effects) when compared with systems formed by tightly bound projectiles, and the most strongly bound nuclei included in the systematics, the ^{4}He and ^{12}C system, present a lowering of the reduced reaction cross sections, possibly due to their structure, which may cause reaction channels to be closed.

ACKNOWLEDGMENTS

The authors thank Professor J. Lubián (UFF) for his valuable suggestions in the theoretical analysis, Professor W. Seale for the corrections on the text, and the Conselho Nacional de Pesquisa e Desenvolvimento (CNPq) and the Fundação de Amparo à Pesquisa do Estado de São Paulo (FAPESP) for support.‘

[1] E. Benjamim *et al.*, Phys. Lett. B **647**, 30 (2007).
[2] T. Matsumoto, T. Egami, K. Ogata, Y. Iseri, M. Kamimura, and M. Yahiro, Phys. Rev. C **73**, 051602 (2006).
[3] J. Lubian, T. Correa, E. F. Aguilera, L. F. Canto, A. Gomez-Camacho, E. M. Quiroz, and P. R. S. Gomes, Phys. Rev. C **79**, 064605 (2009).
[4] A. Barioni *et al.*, Phys. Rev. C **80**, 034617 (2009).
[5] E. F. Aguilera *et al.*, Phys. Rev. C **63**, 061603 (2001).
[6] P. N. de Faria *et al.*, Phys. Rev. C **81**, 044605 (2010).
[7] P. R. S. Gomes, J. Lubian, I. Padron, and R. M. Anjos, Phys. Rev. C **71**, 017601 (2005).
[8] L. Canto, P. Gomes, J. Lubian, L. Chamon, and E. Crema, Nucl. Phys. A **821**, 51 (2009).
[9] J. Shorto, P. Gomes, J. Lubian, L. Canto, S. Mukherjee, and L. Chamon, Phys. Lett. B **678**, 77 (2009).
[10] E. F. Aguilera, I. Martel, A. M. Sánchez-Benítez, and L. Acosta, Phys. Rev. C **83**, 021601 (2011).
[11] A. Barioni *et al.*, Phys. Rev. C **84**, 014603 (2011).
[12] R. Lichtenthäler *et al.*, Eur. Phys. J. A **25**, 733 (2005).
[13] L. Jarczyk, J. Okolowicz, A. Strzalkowski, K. Bodek, M. Hugi, L. Lang, R. Muller, and E. Ungricht, Nucl. Phys. A **316**, 139 (1979).
[14] I. J. Thompson, Comput. Phys. Rep. **7**, 167 (1988).
[15] L. C. Chamon, B. V. Carlson, L. R. Gasques, D. Pereira, C. De Conti, M. A. G. Alvarez, M. S. Hussein, M. A. Cândido Ribeiro, E. S. Rossi, and C. P. Silva, Phys. Rev. C **66**, 014610 (2002).
[16] M. A. G. Alvarez, L. C. Chamon, M. S. Hussein, D. Pereira, L. R. Gasques, E. S. Rossi Jr., and C. P. Silva, Nucl. Phys. A **723**, 93 (2003).
[17] B. Kamys, L. Jarczyk, Z. Rudy, A. Strzalkowski, H. H. Wolter, J. Lang, R. Muller, and J. Sromicki, Nucl. Phys. A **406**, 193 (1983).
[18] C. M. Perey and F. G. Perey, At. Data Nucl. Data Tables **17**, 1 (1976).
[19] N. Keeley, K. W. Kemper, and K. Rusek, Phys. Rev. C **64**, 031602 (2001).
[20] T. Matsumoto, E. Hiyama, K. Ogata, Y. Iseri, M. Kamimura, S. Chiba, and M. Yahiro, Phys. Rev. C **70**, 061601 (2004).
[21] K. C. C. Pires *et al.*, Phys. Rev. C **83**, 064603 (2011).
[22] [http://www.nndc.bnl.gov/].
[23] D. Tilley, J. Kelley, J. Godwin, D. Millener, J. Purcell, C. Sheu, and H. Weller, Nucl. Phys. A **745**, 155 (2004).
[24] J. M. B. Shorto, E. Crema, R. F. Simões, D. S. Monteiro, J. F. P. Huiza, N. Added, and P. R. S. Gomes, Phys. Rev. C **78**, 064610 (2008).
[25] M. J. Rhoades-Brown and P. Braun-Munzinger, Phys. Lett. B **136**, 19 (1984).
[26] A. Diaz-Torres and I. J. Thompson, Phys. Rev. C **65**, 024606 (2002).
[27] J. E. Poling, E. Norbeck, and R. R. Carlson, Phys. Rev. C **5**, 1819 (1972).
[28] J. E. Poling, E. Norbeck, and R. R. Carlson, Phys. Rev. C **13**, 648 (1976).
[29] D. E. Trcka, A. D. Frawley, K. W. Kemper, D. Robson, J. D. Fox, and E. G. Myers, Phys. Rev. C **41**, 2134 (1990).
[30] R. E. Warner *et al.*, Phys. Rev. C **51**, 178 (1995).
[31] R. J. Smith, J. J. Kolata, K. Lamkin, A. Morsad, K. Ashktorab, F. D. Becchetti, J. A. Brown, J. W. Janecke, W. Z. Liu, and D. A. Roberts, Phys. Rev. C **43**, 761 (1991).
[32] L. Jarczyk, B. Kamys, A. Strzałkowski, A. Szczurek, M. Godlewski, J. Lang, R. Müller, and J. Sromicki, Phys. Rev. C **31**, 12 (1985).
[33] A. T. Rudchik *et al.*, Nucl. Phys. A **695**, 51 (2001).
[34] E. B. Carter, G. E. Mitchell, and R. H. Davis, Phys. Rev. **133**, B1421 (1964).
[35] R. J. Ledoux, M. J. Bechara, C. E. Ordonez, H. A. Al-Juwair, and E. R. Cosman, Phys. Rev. C **27**, 1103 (1983).
[36] C. Y. Wong, Phys. Rev. Lett. **31**, 766 (1973).